Plasma Chem Plasma Process (2018) 38:207–222
https://doi.org/10.1007/s11090-017-9862-2

ORIGINAL PAPER

Analytical Analysis of Different Karats of Gold Using Laser Induced Breakdown Spectroscopy (LIBS) and Laser Ablation Time of Flight Mass Spectrometer (LA-TOF-MS)

Nasar Ahmed[1,2] · Rizwan Ahmed[1] · M. Aslam Baig[1]

Received: 7 September 2017 / Accepted: 13 November 2017 / Published online: 18 November 2017

Abstract Laser induced breakdown spectroscopy (LIBS) coupled with a laser ablation time of flight mass spectrometer (LA-TOF-MS) has been developed for discrimination/analysis of the precious gold alloys cartage. Five gold alloys of Karats 18K, 19K, 20K, 22K and 24K having certified composition of gold as 75, 79, 85, 93 and 99.99% were tested and their precise elemental compositions were determined using the laser produced plasma technique. The plasma was generated by focusing beam of a Nd:YAG laser on the target in air and its time integrated emission spectra were registered in the range 250–870 nm. The calibration free LIBS technique (CF-LIBS) was used for the quantitative determination of the constituent elements present in different Karats of gold. Elemental compositions of these gold alloys were also determined using a Laser Ablation time of flight mass spectrometer (LA-TOF-MS). The LIBS limit of detection was calculated from the calibration curves for copper, silver and gold. Results of CF-LIBS and LA-TOF-MS are in excellent agreement with the certified values. It is demonstrated that LIBS coupled with LA-TOF-MS is an efficient technique that can be used to analyze any precious alloys in a fraction of a second.

Keywords LIBS · Karats of gold · Elemental composition · Plasma parameters · LA-TOF-mass spectrometry

✉ M. Aslam Baig
baig@qau.edu.pk; baig77@gmail.com

[1] National Centre for Physics, Quaid-i-Azam University Campus, Islamabad 45320, Pakistan

[2] Department of Physics, University of Azad Jammu and Kashmir, Muzaffarabad 13100, Pakistan

Introduction

Gold is a soft, reddish yellow, shiny and precious metal, being extensively used in Ornaments, Jewelry, Medals, Electronics and Finances. China, Russia, the United States are the world dominant gold producing countries with massive reserves. Precise determination of elemental composition in different Karats of gold is an attractive subject in gold mining industry as its composition must meet the international standards. Therefore, certification of the cartage of gold alloys is always a challenging and demanding process. The standard methods used for the identification of different Karats of gold are accurate but there are several drawbacks associated with the traditional methods. These methods are unwieldy, destructive and require preliminarily information about the gold percentage in the sample. The information about the Karat is only possible for the newly made jewelry but for the unknown Karats of jewelry, a repetitive analysis is necessary to get exact information about the gold percentage [1, 2].

To resolve the above-mentioned problems, several techniques have been employed [3, 4]. Among these techniques, XRF, LIBS and LA-TOF-MS are the non-distractive techniques. LIBS and XRF [5–7] provides limits of detection in the order of parts per million. In the XRF analysis, the surface of the jewelry needs to be flat and sufficiently large. However, for the analysis of gold ornaments and jewelry it is impossible to use this technique. Besides, XRF can only provide 1–2 μm depth profiling, so this technique is not advantageous for the gold stuff having surface treatments [4].

To overcome these problems for the gold alloy composition determination, we combined the laser induced breakdown spectroscopy (LIBS) [8–10] and laser ablation time of flight mass spectrometry (LA-TOF-MS) [11–17] techniques. Laser ablation is a good alternate to the above-mentioned techniques due to its superior limit of detection and batter depth profiling capability. Laser produce plasma induces crater with diameter up to 100 of micrometers and depth of more than 10 μm depending upon the laser beam profile, focusing optics and laser energy [17]. Any material holding any shape can be easily analyzed using this technique. As LIBS is a non-distractive technique and its portable versions are also available, therefore this technique can be used for quality control in industries [17–19]. Due to these features, LIBS technique has advantages over the other standard techniques. Calibration curve LIBS technique has been hardly used for accurate analysis of gold Karats due to the matrix effect, self-absorption and other experimental uncertainties. In the calibration free LIBS approach all the elements of the sample can be detected, and it requires no external standards for calibration. However, CF-LIBS [20–22] is useful only in the case where the plasma is optically thin [17] and is in the local thermodynamically equilibrium (LTE) [23–25]. This method has been successfully applied for the compositional analysis of precious alloys [26], gases and archeological samples [27] and cartage analysis [28]. Provided the optically thin and LTE conditions are satisfied for all the lines, this method can be used to get accurate compositional analysis [20]. If self-absorption is present, then errors are bound to appear. To improve the CF-LIBS results, an internal reference self-absorption correction (IRSAC) method [29, 30] was proposed to correct the emission line intensities with reference to an internal standard line.

In the present work, we have utilized the calibration free CF-LIBS technique to analyze the LIBS spectra for precious alloy compositions without any external calibrations. All the five different Karats (18K, 19K, 20K, 22K and 24K) having certified composition of gold as 75, 79, 85, 91 and 99.9% were also analyzed using a Laser Ablation Time of Flight Mass Spectrometer (LA-TOF-MS). The LIBS limit of detection (LOD) was calculated for Cu and Ag in the gold alloys by normalizing the emission line intensities of each element by

the emission line intensity of gold to reduce the effect of instrumental error and signal fluctuations. It is demonstrated that LIBS and LA-TOF-MS yields accurate and complementary compositional results for precise Karats compositions of precious alloys.

Experimental

The experimental details for recording the optical emission spectrum of the laser produced plasma is the same as described in our earlier papers [31–34]. In brief, the laser produced gold alloy plasma was generated using a high-power Q-switched Nd:YAG Laser (Brilliant-B Quantel, France), 5 ns pulse duration and 10 Hz repetition rate, capable of delivering pulse energy up to 850 mJ at 1064 nm and 500 mJ at 532 nm. The laser pulse energy was varied by varying the Q-switch delay. A quartz lens (convex) of 20 cm focal length was used to focus the laser beam on the target sample placed in air at atmospheric pressure. The laser pulse energy was varied from 80 to 120 mJ and the measured diameter of the focused laser beam was about (0.10 ± 0.01) cm (laser fluence about 10–15 J/cm^{-2}). The laser energy was measured by an energy meter (Nova-Quantel, France). To prevent the formation of deep craters, the sample was placed on a rotating stage for providing fresh surface of the target to every laser shot. In order to prevent the air breakdown in front of the sample, it was necessary to keep the distance between the lens and the sample less than the focal length. An optical fiber (high –OH, core diameter about 600 μm) was used to collect the plasma radiation with a collimating lens (0°–45° field of view) which was placed normal to the laser beam. The emitted radiation was captured by a set of four spectrometers (Avantes, Hollands) each having 10 μm slit width and covering the wavelength range of 250–870 nm. To correct the emission signal, the dark signal was subtracted from the observed signal using the LIBS software.

The same gold samples were also qualitatively as well as quantitatively analyzed by using a Laser-ablation Time of Flight Mass Spectrometer (LA-TOF-MS) [35] however, the laser fluence was much lower; in the range of (0.1–1) J/cm^2. This system is integrated with three electrodes in rectangular shapes (3 cm × 3 cm), two of the electrodes hold 1 cm openings in the center which is covered with fine tungsten mesh and detection system at 100 cm from the extraction region. The entire system was coupled with a turbo molecular pump backed by a mechanical pump to maintain vacuum at about 2 × 10^{-6} mbar during the experiment. The laser beam was focused by a quartz lens of 30 cm focal length which was placed in front of the entrance window of the vacuum chamber. The generated ions were detected by a channeltron, operating at a voltage of 2 kV. The ion signal was analyzed by a 500 MHz digital storage oscilloscope (Tektronix) coupled with a personal computer.

Emission Studies

The LIBS spectrum consists of spectral lines of the constituent elements which gives information about the major and trace elements present in the sample. The intensities of the observed spectral lines are proportional to their concentrations. The plasma at the surfaces of different gold alloys was generated by focusing the Nd: YAG laser beam with pulse energy of about 400 mJ at 532 nm. As soon as the plasma is generated, the plasma plume expands perpendicular to the target surface and after a few micro seconds, it cools down

and emits the characteristics spectra of the constituent elements. Typical spectra of five different Karats (18K, 19K, 20K, 22K and 24K) of gold produced plasma produced by focusing a 100 mJ and 5 ns laser pulse at 532 nm (Laser fluence about 12 J/cm^2) are shown in Fig. 1a, b covering the wavelength region from 250 to 870 nm. The characteristic lines of gold, silver and copper are evident that are labeled in the figure corresponding to their wavelengths. The resonance lines of Au, Ag and Cu are observed which facilitates the identifications of the observed spectra. The advantage of studying laser produced plasma in air at an atmospheric pressure is that it keeps the plasma confined, LTE condition can be achieved within a couple of microseconds after the production of plasma and the spectral lines of hydrogen, oxygen and nitrogen also appear which can be used for the plasma diagnostics. However, it will not affect the relative compositional analysis of the samples.

In Fig. 2 we show the emission spectra of gold alloys in the range 508–548 nm, showing variations in the emission line intensities of Cu I lines at 510.29, 515.32 and 521.82 nm, Ag I lines at 520.90 and 546.55 nm, Au I at 523.026 nm with different Karat of the gold. The observed line intensities of copper, silver and gold are in accordance to the Karats of the gold samples, the larger the concentration the higher the line intensity. The

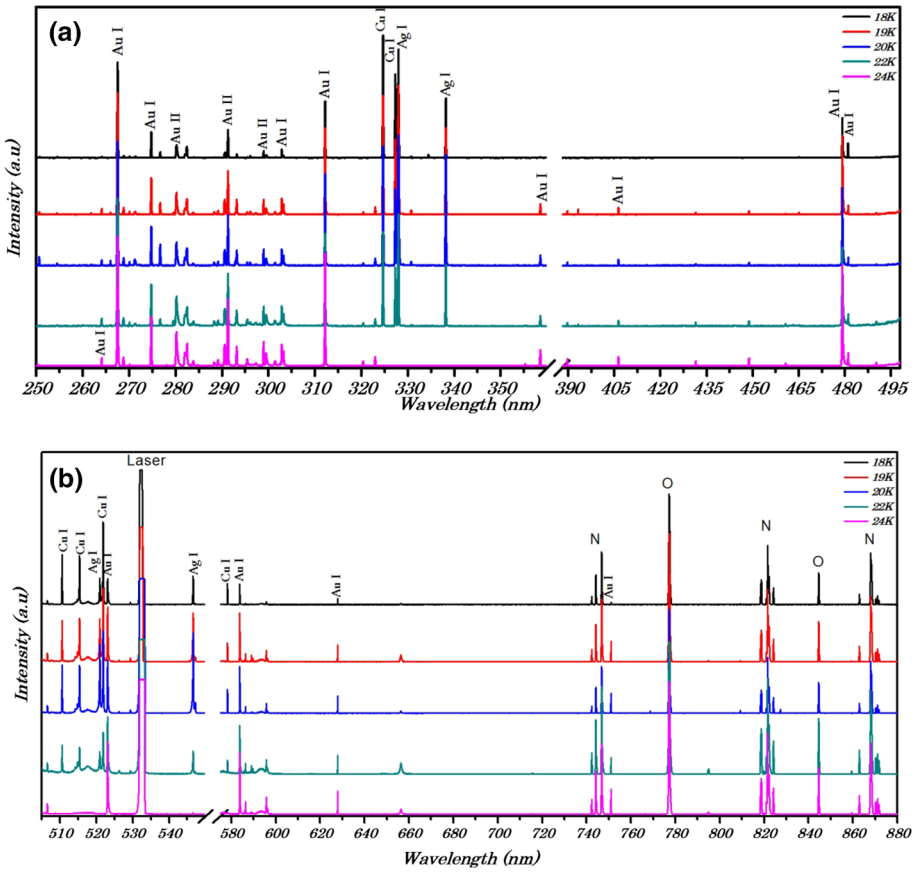

Fig. 1 (Color online) Typical optical emission spectra of the laser produced plasmas at the gold alloys, 24K, 22K, 20K, 19K and 18K, covering the spectral region 250–870 nm, using laser energy 100 mJ and 2 μs time delay

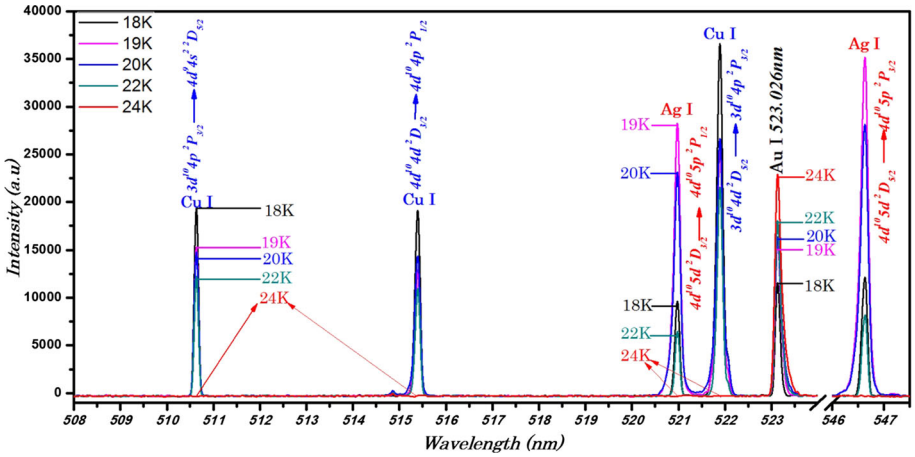

Fig. 2 (Color online) Emission spectra of the laser produced plasmas of different Karat of the gold covering the spectral region 508–547 nm showing variations in the line intensities of copper, silver and gold

spectrum of the 24 Karat gold shows only the gold lines and not a single line of silver and copper is present which guarantees the quality and purity of the gold sample.

Determination of Plasma Temperature

The plasma temperature was calculated from the relative line intensities of Cu, Ag and Au using the Boltzmann plot method. The spectral lines used to construct the Boltzmann Plot are listed in the Table 1 along with the other spectroscopic parameters taken from the Literature [36–41]. Errors are bound to be present in the determination of the plasma temperature by the Boltzmann plot method due to the uncertainties in the transition probabilities and measured line intensities. Therefore, the determined plasma temperature comprises about 10% error. Absorption of photons within the laser-induced plasma may cause self-absorption and it will be more evident in the emission lines where the lower level of transition is equal or close to the ground state. The effect of self-absorption apparently reduces the peak intensity and line broadening. If the self-absorption contribution is large, a self-reversal dip appears at the top of the line which is a sign of a strongly inhomogeneous plasma. Even slightly self-absorbed lines used in the CF-LIBS method may cause error in determining the compositions. However, in the present experimentation there was not a single line which shows such a distorted line profile. On the safe side and to minimize such minor effects of self-absorption, we have corrected the observed line intensities of Cu, Ag and Au for self-absorption [29, 30] but this correction is much lower than 10%.

Figure 3 shows typical Boltzmann plots of the 22K gold alloy using the intensity corrected neutral Cu lines, singly ionized Ag lines and neutral Au lines. The linarites in the Boltzmann Plots reveals the selection of the appropriate lines to deduce the plasma temperatures. The plasma temperature estimated from the Cu I lines was (9500 ± 500) K, Ag II lines (10,500 ± 500) K and Au I lines (10,000 ± 500) K. The average values of the plasma temperatures estimated for the 18K, 19K, 20K and 22K samples are (9800 ± 500) K, (10,300 ± 500) K, (11,000 ± 500) K and (10,000 ± 500) K

Table 1 Spectroscopic parameters of the emission lines of Cu I and Ag II, Au I used to construct the Boltzmann plots

Wavelength λ (nm)	Transition			Transition probability (10^7 s^{-1})	E_k (eV)	g_k
	Upper level		Lower level			
Cu I						
261.84	$3d^{10}5p\ ^2P_{3/2}$	→	$3d^9 4s^2\ ^2D_{5/2}$	3.07	6.12	4
282.43	$3d^9 4s4p\ ^2D_{5/2}$	→	$3d^9 4s^2\ ^2D_{5/2}$	0.78	5.78	6
293.30	$3d^9 4s4d\ ^4G_{7/2}$	→	$3d^9 4s4p\ ^4P_{5/2}$	0.12	9.30	8
296.12	$3d^9 4s4p\ ^2F_{7/2}$	→	$3d^9 4s^2\ ^2D_{5/2}$	0.37	5.57	8
299.73	$3d^9 4s4p\ ^2D_{5/2}$	→	$3d^9 4s^2\ ^2D_{3/2}$	0.12	5.78	6
324.75	$3d^{10}4p\ ^2P_{3/2}$	→	$3d^{10}4s\ ^2S_{1/2}$	13.9	3.82	4
327.39	$3d^{10}4p\ ^2P_{1/2}$	→	$3d^{10}4s\ ^2S_{1/2}$	13.7	3.79	2
330.79	$3d^9 4s4d\ ^4G_{11/2}$	→	$3d^9 4s4p\ ^4F_{9/2}$	22.2	8.82	12
465.11	$3d^9 4s5s\ ^4D_{7/2}$	→	$3d^9 4s4p\ ^4F_{9/2}$	3.80	7.74	8
510.55	$3d^{10}4p\ ^2P_{3/2}$	→	$3d^9 4s^2\ ^2D_{5/2}$	0.20	3.82	4
515.32	$3d^{10}4d\ ^2D_{3/2}$	→	$3d^{10}4p\ ^2P_{1/2}$	6.0	6.19	4
521.82	$3d^{10}4d\ ^2D_{5/2}$	→	$3d^{10}4p\ ^2P_{3/2}$	7.5	6.19	6
529.25	$3d^9 4s5s\ ^4D_{7/2}$	→	$3d^9 4s4p\ ^4D_{7/2}$	1.09	7.74	8
570.02	$3d^{10}4p\ ^2P_{3/2}$	→	$3d^9 4s^2\ ^2D_{3/2}$	0.02	3.82	4
578.21	$3d^{10}4p\ ^2P_{1/2}$	→	$3d^9 4s^2\ ^2D_{3/2}$	0.16	3.79	2
809.26	$3d^{10}5s\ ^2S_{1/2}$	→	$3d^{10}4p\ ^2P_{3/2}$	4.59	5.35	2
Ag II						
250.71	$4d^9 5d\ ^2[1/2]_1$	→	$4d^9 5p\ ^2[3/2]_2$	9.00	16.21	3
266.04	$4d^9 5p\ ^2[3/2]_1$	→	$4d^9 5s\ ^2[3/2]_2$	1.51	10.37	3
276.75	$4d^9 5p\ ^2[7/2]_3$	→	$4d^9 5s\ ^2[3/2]_2$	1.01	10.19	7
283.76	$4d^9 6s\ ^2[3/2]_1$	→	$4d^9 5p\ ^2[3/2]_1$	0.40	15.51	3
289.63	$4d^9 6s\ ^2[3/2]_2$	→	$4d^9 5p\ ^2[3/2]_2$	8.40	15.55	5
822.48	$4d^8 5s5p\ ^5G_4$	→	$4d^9 6s\ ^2[5/2]_3$	0.17	16.45	9
825.48	$4d^9 6p\ ^2[5/2]_3$	→	$4d^9 6s\ ^2[5/2]_2$	1.40	16.49	7
843.15	$4d^9 7s\ ^2[3/2]_1$	→	$4d^9 6p\ ^2[3/2]_1$	2.40	18.48	3
Au I						
264.15	$5d^9 6s6p\ ^2P_{3/2}$	→	$5d^9 6s^2\ ^2D_{5/2}$	3.30	5.83	4
267.59	$5d^{10}6p\ ^2P_{1/2}$	→	$5d^{10}6s\ ^2S_{1/2}$	16.5	4.63	2
268.87	$5d^9 6s6p$ J = 5/2	→	$5d^9 6s^2\ ^2D_{3/2}$	1.34	7.27	6
270.09	$5d^9 6s6p$ J = 5/2	→	$5d^9 6s^2\ ^2D_{5/2}$	0.566	5.72	6
274.83	$5d^9 6s6p\ ^4F_{7/2}$	→	$5d^9 6s^2\ ^2D_{5/2}$	4.82	5.65	8
288.34	$5d^9 6s6p\ ^4D_{3/2}$	→	$5d^9 6s^2\ ^2D_{3/2}$	0.94	6.96	4
302.92	$5d^9 6s6p\ ^4P_{5/2}$	→	$5d^9 6s^2\ ^2D_{5/2}$	0.80	5.23	6
312.28	$5d^{10}6p\ ^2P_{3/2}$	→	$5d^9 6s^2\ ^2D_{5/2}$	1.92	5.11	4
322.60	$5d^{10}10d\ ^2D_{3/2}$	→	$5d^{10}6p\ ^2P_{3/2}$	0.106	8.95	4
406.51	$5d^{10}6d\ ^2D_{3/2}$	→	$5d^{10}6p\ ^2P_{1/2}$	8.35	7.68	4
479.26	$5d^{10}6d\ ^2D_{5/2}$	→	$5d^{10}6p\ ^2P_{3/2}$	8.90	7.69	6
481.16	$5d^{10}6d\ ^2D_{3/2}$	→	$5d^{10}6p\ ^2P_{3/2}$	1.51	7.68	4
583.74	$5d^{10}7s\ ^2S_{1/2}$	→	$5d^{10}6p\ ^2P_{1/2}$	2.64	6.76	2
627.82	$5d^{10}6p\ ^2P_{1/2}$	→	$5d^9 6s^2\ ^2D_{3/2}$	0.337	4.63	2
751.07	$5d^{10}7s\ ^2S_{1/2}$	→	$5d^{10}6p\ ^2P_{3/2}$	3.92	6.76	2

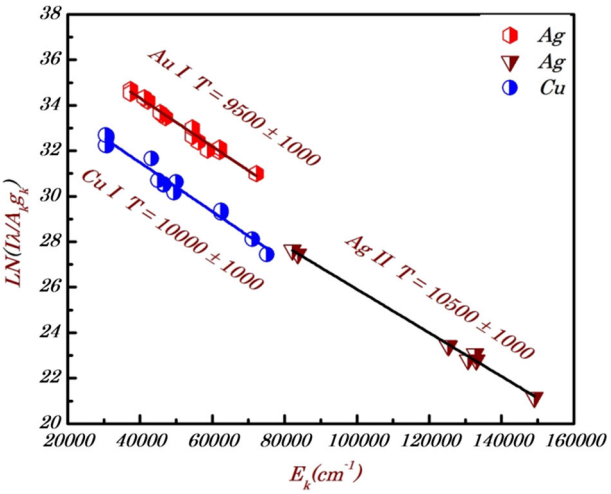

Fig. 3 (Color online) Boltzmann plots of the 22K gold alloy using emission lines of Cu I, Ag II and Au I, Laser pulse energy 100 mJ and 2 μs time delay

respectively. These average apparent plasma temperatures, determined for each gold alloy, were used to estimate the elemental compositions of different Karat of gold alloys. We have determined the plasma temperatures using the neutral lines of copper and gold as well as the ionic lines of silver and interestingly the deduced plasma temperatures are comparable with in the quoted uncertainties. However, the plasma temperature deduced from the ionic lines are slightly higher than that of the neutral lines. This fact was reported by Aguilera et al. [42, 43] who attributed the difference between the plasma temperatures determined from the neutral and ionic lines to the inhomogeneity in the laser produced plasma. It was further inferred that different apparent excitation temperatures for neutral and ionic lines are due to the population-average of the local electronic temperature in the plasma. A more appropriate name of excitation/plasma temperature was suggested as "apparent plasma temperature" which refers to the local plasma temperature for the spatially-integrated measurements. Our results also show a similar trend of the apparent plasma temperatures determined from the neutral and ionic lines.

Determination of Electron number density

In order to estimate the electron number density, we selected the Stark broadened and a well isolated Ag I line at 328.07 nm and the Stark broadened line profile of the hydrogen H_α at 656.28 nm. The width $\Delta\lambda_{FWHM}$ of these lines were determined by de-convoluting the observed line profiles as a Voigt profile, which takes into account the Instrumental width, the Doppler width and the Stark broadening. The instrumental width of our spectrometer is about 0.06 ± 0.01 nm whereas, the Doppler width is about 0.005 nm. The Stark width is related to the electron number density as [44]:

$$n_e = \left(\frac{\Delta\lambda_{FWHM}}{2\omega_s}\right) \times 10^{16} \quad (1)$$

Here, $\Delta\lambda_{FWHM}$ is the full width at half maxima and ω_s is the Stark broadening parameter, which is slightly wavelength and temperature dependent.

In Fig. 4a we show the Stark broadened line profile of the Ag I line at 328.07 nm. The spectrum was recorded using a Nd:YAG laser at 532 nm with pulse energy 100 mJ and at about 2 μs time delay between the laser pulse and the data acquisition system. The dots are the experimental data points and the full line is the Voigt fit, yielding FWHM as (0.11 ± 0.01) nm. The Stark broadening parameter for this line is reported in the literature as 4.65×10^{-2} nm [45]. The electron number density is thus calculated using Eq. 1 as $(2.0 \pm 0.3) \times 10^{17}$ cm^{-3} which includes the errors associated with the extracted FWHM and that in the Stark broadening parameter.

Calculations of the full width at half area of hydrogen H_α line at 656.28 nm is presented in Fig. 4b showing the experimentally observed line profile bounded by two vertical lines representing FWHA as (0.86 ± 0.08) nm. The electron density is calculated using the relation [46, 47]:

$$FWHA = 0.549\,\text{nm} \times \left(\frac{n_e}{10^{23}\text{m}^{-3}}\right)^{0.67965} \quad (2)$$

The electron number density is deduced as $(1.9 \pm 0.5) \times 10^{17}$ cm^{-3}. A good agreement between the number densities derived from the Stark Broadening parameter of Ag I line at 328.07 and hydrogen H_α line is observed. Average values of the number densities were used, see below, to determine the compositions of the samples using CF-LIBS. The electron number density for the gold alloys is estimated in the range $(1–3 \pm 0.5) \times 10^{17}$ cm^{-3} which is subsequently used to calculate the compositions of the elements.

In order to use the LIBS spectra for the quantitative analysis, it is necessary that the laser produced plasma should be optically thin and also satisfies the Local Thermodynamic Equilibrium (LTE) condition. To validate the condition for the optically thin [12, 15, 17], the corrected line intensities of various emission lines of Cu, Ag and Au were compared with the ratio of their transition probabilities [32, 48] which are in agreement within 10%. To check the local thermodynamic equilibrium (LTE), a criteria proposed by McWhirter has been validated for the Au I line at 267.59 nm, Ag I at 328.06 nm and Cu I at 324.75 nm lines. The lower limit for the electron density is calculated using the relation [23]:

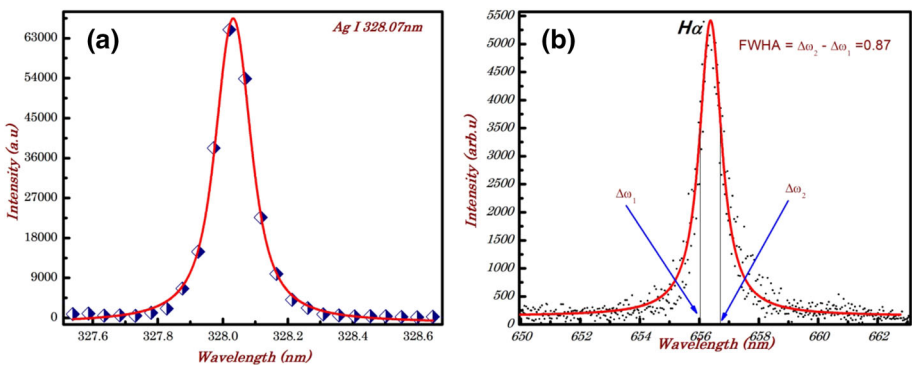

Fig. 4 (Color online) Stark broadened line profile of Ag I line at 328.07 nm (**a**), Calculation f full width at half area of hydrogen H_α line at 656.28 nm at 100 mJ laser energy (**b**)

$$N_e > 1.6 \times 10^{12} \times \Delta E^3 \times T^{1/2} \quad (3)$$

Here, ΔE is the cupper and the lower energy level and T is the excitation temperature. The lower limit for electron densities, calculated from the emission lines of Au I at 267.59 nm, Ag I at 328.06 nm and Cu I at 324.75 nm were in the range of (0.5–1.5 ± 0.5) × 10^{14} cm^{-3} respectively. Evidently, the number densities obtained from the McWhirter criteria are much lower than that determined using the Stark broadening parameters, which are in the range (1–3 ± 0.5) × 10^{17} cm^{-3}. Thus the plasma may be considered close to LTE.

In addition to the McWhirter criterion for stationary and homogeneous plasma, the condition of the validity of LTE in an inhomogeneous plasma was also validated using the spectral lines of gold, copper and silver. The diffusion length λ was calculated using the relation [24, 25]:

$$\lambda \approx 1.4 \times 10^{12} \times \left(\frac{(kT)^{3/2}}{n_e}\right) \times \left(\frac{\Delta E}{M_A f_{12}(\bar{g})}\right)^{1/2} \times e^{\Delta E/2kT} \quad (4)$$

The diffusion length λ is calculated as 0.001 cm, much larger than the characteristic variation length "*d*" equal to 0.2 cm, which is in accordance to the criteria i.e. $10\lambda < d$. In the light of the above conditions it can be safely assumed that the plasma is very close to LTE.

Calibration Free LIBS for Quantitative Analysis

The composition analysis from the observed emission spectra is based on the Boltzmann Plots. However, the accuracy in the calculations of plasma temperatures and intercepts is largely influenced by the self-absorption effect [29, 30]. After correcting the line intensities, the Boltzmann plots were drawn as shown in Fig. 3. Evidently, after incorporating the self-absorption corrections, the data points in the Boltzmann Plot follow a more realistic linear trend and yields more accurate plasma temperature and compositions [29]. For the quantitative determination of the constituents of Cu, Ag and Au in gold alloys, the Boltzmann relation was used which links the intensities of the lines emitted by the same element through the relation [21, 22]:

$$I = FC^s A_k \frac{hc}{\lambda_k} \frac{g_k}{P(T)} \exp\left[-\frac{E_k}{k_B T}\right] \quad (5)$$

where *I* is the emission line intensity, C^s is the composition of the emitting atomic species, F is an experimental factor which takes into account the collection efficiency of the system and P(T) is the partition function. Taking the logarithm on the both sides of Eq. 5

$$\ln\left[\frac{\overline{I_{ba}}}{A_{ba} g_b}\right] = -\frac{E_b}{k_\beta T} + \ln\left[\frac{FC_s}{P(T)}\right] \quad (6)$$

This equation can be compared with a straight-line equation yielding:

$$y = \ln\left[\frac{\overline{I_{ba}}}{A_{ba} g_b}\right], x = E_b, m = -\frac{1}{Tk_B}, \; q_s = \ln\left[\frac{FC_s}{P(T)}\right] \quad (7)$$

Here, q_s is the intercept along the Y-axis of the Boltzmann Plot and its slop m is related to the plasma temperature. If the laser produced plasma is close to LTE then the slops of the Boltzmann plots for each element should be approximately the same but the intercepts may differ according to the concentration of that element in the sample. Simplifying Eq. 7, we can determine the Experimental Factor and the elemental concentration using the following relation [48]:

$$FC^s = P(T) \times e^{q_s} \tag{8}$$

Here, F is the experimental factor and q_s is the intercept on the Y-axis of the Boltzmann plot. The values of C^{Cu}, $C^{Ag,}$ and C^{Au} were estimated as follows:

$$C^s = \frac{P(T) \times e^{q_s}}{F} \tag{9}$$

Due to the insufficient lines of ionized gold and copper and neutral lines of silver, it was not probable to draw the Boltzmann plots. Thus, the Saha-Boltzmann equation [49] was used to determine the compositions of the ionized species of gold and copper and neutral species for silver. The total concentration of an element is the sum of the concentration of both, neutral and the ionize species. By adopting the above procedure, the composition of the 18K gold alloy was obtained as 75% Au, 21% Cu, 4% Ag, 19K gold alloy as 79% Au, 7% Cu, 12% Ag, 20K gold alloy as 83% Au, 6% Cu, 11% Ag, and 22K gold alloy as 93% Au, 5% Cu, and 2% Ag. The calibration free LIBS technique yields improved percentage compositions of these gold alloys. The errors attached in this procedure are less than 10%.

Limits of Detection

The lines possessing much higher intensities are good candidates for the determination of the limit of detection (LOD) as compared to the weaker emission lines [50, 51]. To draw the calibration curves, the line intensities of copper and silver were normalized by the intensity of the gold line at 312.28 nm to reduce the effect of the instrumental signal fluctuations and matrix effects. The calibration curves of copper and silver were drawn and the normalized intensity versus the relative compositions for the five gold alloys are presented in Fig. 5a, b. The error bars show the calculated standard deviations of the signal intensities for copper and silver. All the calibration curves were drawn for the data collected at 100 mJ laser energy operating at 532 nm with 5 ns pulse duration. The calibration curves show good linearity, R^2 i.e. correlation factor for the linear fit of copper and silver is 0.99 within the experimental uncertainty. The calibration curve for gold is also drawn with the intensities of the neutral gold lines at 479.26 and at 523.02 nm against the gold concentration in Fig. 5.

All the samples were validated reasonably well with the actual/certified concentrations in the gold alloys, which shows the quality of the fitting. The limit of detection is calculated using the equation [52].

$$LOD = \frac{3\sigma}{b} \tag{10}$$

where σ is the standard deviation of the background and b is the slope of the calibration curve. To calculate σ, more than hundred background noise values were taken on both the sides of the peaks from the spectrum. The LOD values obtained for Cu, Ag and Au are

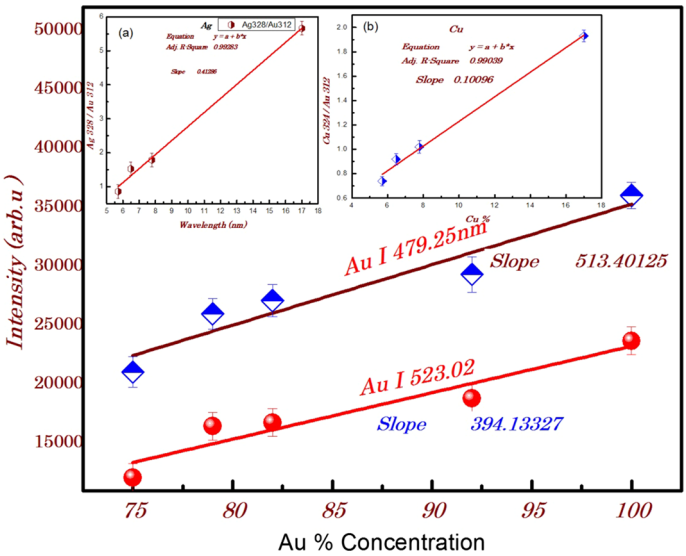

Fig. 5 (Color online) Calibration curves of copper and silver obtained by drawing the normalized line intensities against concentrations. The calibration curves for gold were drawn using the neutral gold lines at 479.26 nm and at 523.02 nm. The error bars show the standard deviations for the measured signal intensities

17.75, 4.3 and 0.05 ppm respectively, which are in good agreement with the reported values in the literature [50–53]. The high value of LOD in copper is attributed to the energy transfer between the elements within the matrix [50].

Compositional Analysis Using Laser Ablation Time of Flight Mass Spectrometer (LA-TOF-MS)

Compositional analysis of all the Karats of gold alloys were also performed using a locally fabricated laser ablation Time of Flight Mass Spectrometer (LA-TOF-MS) [35]. The spectra of all the samples acquired on the LA-TOF-MS using a Nd:YAG laser (532 nm) at laser fluence in the range of 0.1–1 J/cm^{-2} and at 2 kV channeltron voltage is shown in Fig. 6.

The peaks appeared at m/z = 63, 107 and at 197 correspond to copper, silver and gold respectively. The isotopic peaks of Cu (Cu^{63}, Cu^{65}) and silver (Ag^{107}, Ag^{109}) are not clear in this figure, although we have resolved these isotopic peaks in a separate experiment. The dominating peak at m/z = 197 corresponds to gold, the peak heights of copper and silver appear in accordance to their concentrations/composition in the samples.

In Fig. 7, we present an enlarged portion of the spectra showing variations in the line intensities of the mass spectra with different Karats of the gold with Lorentz fit to the experimental data points. As 24K comprise of 99.99% gold therefore, the time of flight mass spectrum shows only one peak, appeared at m/z = 197. The relative mass composition/abundance of copper, silver and gold were carried out by using the integrated line intensities. Using this technique, the composition of 18K gold alloy was obtained as 17% copper, 7.1% silver and 75.9% gold. The 19K gold alloy consists of 7.78% copper, 13.58% silver, and 78.64% gold. The 20K gold alloy contains about 6.48% copper, 11.42% silver

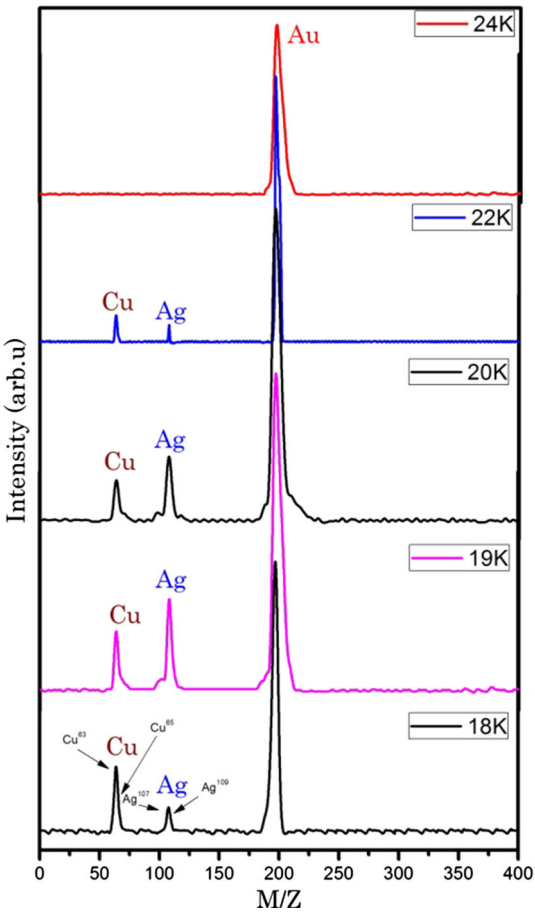

Fig. 6 (Color online) Laser ablation time of flight mass spectra of 24K, 22K, 20K, 19K and 18K gold alloys at 5 mJ Laser pulse energy

and 82% gold. The 22K gold alloy consists of 5.7% copper, 1.6% silver and 92.7% gold whereas, 24K pure gold having 99.99% purity and consequently no other peak of any element was detected in the spectrum.

In Fig. 8 we present a bar graph showing the variations in the compositional analysis results using the calibration free laser induced breakdown spectroscopic technique (CF-LIBS) and the laser ablation time of flight mass spectroscopic (LA-TOF-MS) technique for the analysis of the 18, 19, 20 and 22K Karats of gold samples. From the bar graph it is evident that the Au composition by both the techniques shows excellent agreement with the certified composition. About (2–3)% deviation from the certified values have been noticed in these samples.

It is worth to mention that we used the optical emission spectra of the laser produced gold alloys plasma generated in air to determine the relative compositional analysis of the constituent elements. The advantage of studying the laser produced plasma in air that the plasma remains confined and a relatively higher plasma temperature can be achieved and secondly some lines of hydrogen, in particular the Hα line, appear in the spectrum. Since the line profile of the Hα line is free from self-absorption therefore it can be used to deduce a reliable value of the electron number density. The laser produced plasma generated under

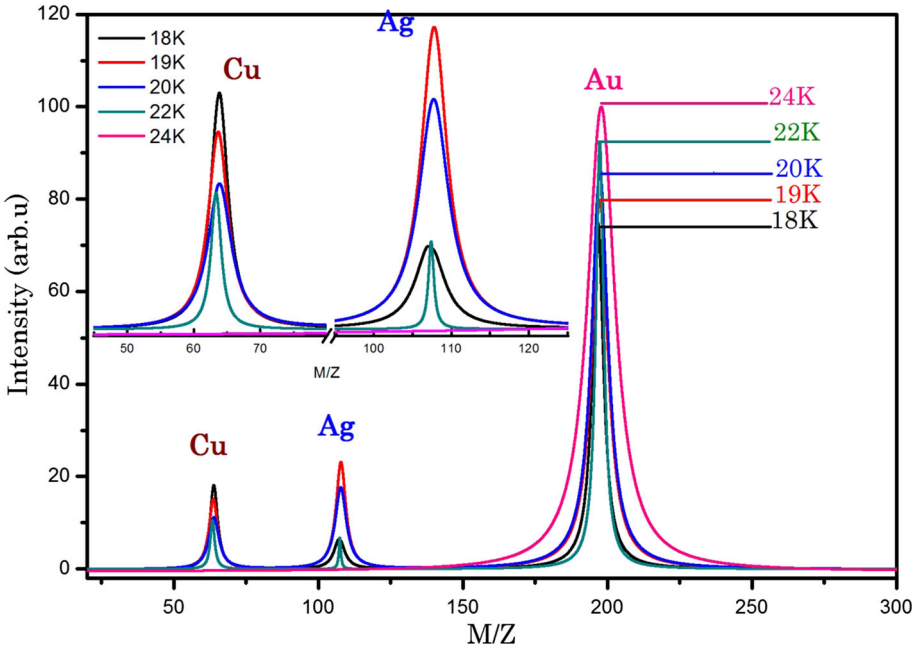

Fig. 7 (Color online) Enlarge spectra with Lorentz fit to the experimental data points of the laser ablation time of flight mass spectra of gold alloy samples

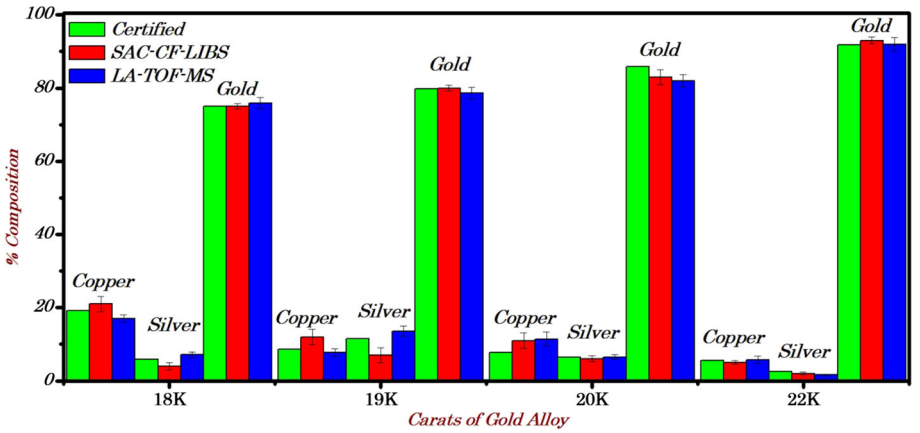

Fig. 8 (Color online) Bar graph showing the agreement of compositional analysis of all Karats of gold by CF-LIBS and LA-TOF-MS

vacuum will expand rather fast and its optical spectrum will also yield equivalent compositional results. The laser-ablation Time of Flight Mass Spectrometer (LA-TOF-MS), which works under high vacuum, has been used to detect the relative concentration of the constituent ions.

Conclusion

We have demonstrated that the calibration free laser induced breakdown spectroscopy (CF-LIBS) combined with a laser ablation time of flight mass spectrometric technique (LA-TOF-MS) is a much advantageous method for the quantitative analysis of gold alloys that yields results with higher accuracy and precision as compared to that of other traditional methods. The other traditional methods require additional information about the Karats prior to the analysis. The conspicuous advantage of the proposed technique is that there is no need to have the preliminary information about the gold content of the sample or about the gold Karats. The linearity of the calibration curves demonstrates a good agreement between the gold Karats and their relative intensities. This method yields a very low limit of detection for gold approximately 0.05 ppm, for silver and copper as 4.3 and 17.75 ppm respectively. Results of CF-LIBS and LA-TOF-MS are in excellent agreement with the certified values which validates the present method for a fast and precise determination of gold in jewelry without any specific sample preparation.

Acknowledgements We are grateful to the Pakistan Academy of Sciences for the financial assistance to acquire the Laser system and for the fabrication of the Laser ablation Time of Flight Spectrometer. The Higher Education Commission of Pakistan gratefully acknowledged for the Indigenous Ph.D. Scholarship to Mr. Nasar Ahmed.

References

1. Derby WG (1917) Furnace methods of assaying for gold and silver. In: Scott WW (ed) Standard methods of chemical analysis. Van Nostrand, New Yrok, pp 739–775
2. Davis JR (1998) Metals handbook. ASM International, Materials Park, pp 624–628
3. Corti CW (2001) Assaying of gold jewellery: choice of technique. Gold Technol 32:20–30
4. Brill M (1997) Analysis of carat gold. Gold Technol 22:10–25
5. Marucco A, Stankiewicz W (1998) Development of an XRF spectrometry analytical method for gold determination in gold jewellery alloys. Gold Technol 24:14–22
6. Marucco A (2004) Low-energy ED-XRF spectrometry application in gold assaying. Nucl Instrum Methods B 213:486–490
7. Honkimaki V, Hamalainen K, Manninen S (1996) Quantitative X-ray fluorescence analysis using fundamental parameters: application to gold jewelry. X-Ray Spectrom 25:215–220
8. Zheng L, Kulkarni P (2017) Rapid elemental analysis of aerosols using atmospheric glow discharge optical emission spectroscopy. Anal Chem 89:6551–6558
9. Lee DH, Han SC, Kim TH, Yun J (2011) Highly sensitive analysis of boron and lithium in aqueous solution using dual-pulse laser-induced breakdown spectroscopy. Anal Chem 83:9456–9461
10. Tsai SJJ, Chen SY, Chung YS, Tseng PC (2006) Spatially resolved, laser-induced breakdown spectroscopy, development, and application for the analysis of Al and Si in nickel-based alloys. Anal Chem 78:7432–7439
11. Griem HR (1964) Plasma spectroscopy. McGraw-Hill Inc, New York
12. Griem HR (1997) Principles of plasma spectroscopy. Cambridge University Press, Cambridge
13. Miziolek A, Palleschi WV, Schechter I (2006) Laser-induced breakdown spectroscopy fundamentals and applications. Cambridge University Press, Cambridge
14. Cremers DA, Radziemski LJ (2006) Handbook of laser-induced breakdown spectroscopy. Wiley, New York
15. Noll R (2012) Laser-induced breakdown spectroscopy—fundamentals and applications. Springer, Heidelberg
16. Kundel ML, Huang RJ, Thorenz UR, Bosle J, Mann MJD, Ries M, Hoffmann T (2012) Application of time-of-flight aerosol mass spectrometry for the online measurement of gaseous molecular iodine. Anal Chem 84:1439–1445
17. Cremers DA, Radziemski LJ (2006) Handbook of laser-induced breakdown spectroscopy. Wiley, New York

18. Noll R, Begemann CF, Brunk M, Connemann S, Meinhardt C, Scharun M, Sturm V, Makowe J, Gehlen C (2014) Laser-induced breakdown spectroscopy expands into industrial applications. Spectrochim Acta Part B 93:41–51
19. Abdulmadjid SN, Marpaung AM, Pardede M, Suliyanti MM, Hidayah AN, Jobiliong E, Lie TJ, Tjia MO, Kurniawan KH (2012) Quantitative analysis of deuterium in zircaloy using double-pulse laser-induced breakdown spectrometry (LIBS) and helium gas plasma without a sample chamber. Anal Chem 84:2224–2231
20. Tognoni E, Cristoforetti G, Legnaioli S, Palleschi V, Salvetti A, Mueller M, Panne U, Gornushkin I (2007) numerical study of expected accuracy and precision in calibration-free laser-induced breakdown spectroscopy in the assumption of ideal analytical plasma. Spectrochim Acta, Part B 62:1287–1302
21. Borgia I, Burgio LMF, Corsi M, Fantoni R, Palleschi V, Salvetti A, Squarcialupi MS, Togoni E (2000) Self-calibrated quantitative elemental analysis by laser-induced plasma spectroscopy: application to pigment analysis. J Cult Herritage 1:281–286
22. Harilal SS, Shay BO, Tillah MS (2005) Spectroscopic characterization of laser-induced tin plasma. J Appl Phys 98:0133061–0133067
23. McWhirter RWP (1965) In: Huddlestone RH, Leonard SL (eds) Plasma diagnostic techniques. Academic, New York
24. Cristoforetti G, De Giacomo A, Dell'Aglio M, Legnaioli S, Togoni E, Palleschi V, Omenetto N (2010) Local thermodynamic equilibrium in laser induced breakdown spectroscopy: beyond the Mcwhirter criterion. Spectrochim Acta, Part B 65:86–95
25. Cristoforetti G, Tognoni E, Gizzi LA (2013) Thermodynamic equilibrium states in laser-induced plasmas: from the general case to laser-induced breakdown spectroscopy plasmas. Spectrochim Acta Part B 90:1–22
26. Rifai K, Laflamme M, Constantina M, Vidal F, Sabsabi M, Blouin A, Bouchardb P, Fytas K, Castello M, Nguegang B (2017) Analysis of gold in rock samples using laser-induced breakdown spectroscopy: matrix and heterogeneity effects. Spectrochim Acta Part B 134:33–41
27. Burakov VS, Raikov SN (2007) Quantitative analysis of alloys and glasses by a calibration-free method using LIBS. Spectrochim Acta, Part B 62:217–223
28. Corsi M, Cristoforetti G, Palleschi V, Salvetti A, Tognoni E (2001) A fast and accurate method for the determination of precious alloys caratage by LIPS. Eur Phys J D 13:373–377
29. Sun L, Yu H (2009) Correction of self-absorption effect in calibration free laser-induced breakdown spectroscopy by an internal reference method. Talanta 79:388–395
30. Sherbini AM, Sherbini TM, Hegazy H, Cristoforetti G, Legnaioli S, Palleschi V, Pardini L, Salvetti A, Tognoni E (2005) Evaluation of self-absorption coefficient of aluminium emission lines in laser induced breakdown spectroscopy measurements. Spectrochim Acta Part B 60:1573–1579
31. Shaikh NM, Rashid B, Hafeez S, Jamil Y, Baig MA (2006) Measurement of ekectron density and temperature of laser induced zinc plasma. J Phys D Appl Phys 39:13841392
32. Ahmed N, Umar ZA, Ahmed R, Baig MA (2017) On the elemental analysis of different cigarette brands using laser induced breakdown spectroscopy and laser-ablation time of flight mass spectrometry. Spectrochim Acta Part B 136:39–44
33. Ahmed N, Ahmed R, Rafiqe M, Baig MA (2016) A comparative study of Cu–Ni alloy using LIBS, LA-TOF, EDX, and XRF. Laser Part Beams 35:1–9
34. Iqbal J, Mahmood S, Tufail I, Asghar H, Ahmed R, Baig MA (2015) On the use of laser induced breakdown spectroscopy to characterize the naturally existing crystal in Pakistan and its optical emission spectrum. Spectrochim Acta Part B 111:80–86
35. Ahmed N, Ahmed R, Umar ZA, Baig MA (2017) Laser ionization time of flight mass spectrometer for isotope mass detection and elemental analysis ofmaterials. Laser Phys 27:086001
36. Hannaford P, Larkins PL, Lowe RM (1981) Radiative lifetimes and branching ratios for the 6^2P_0 levels of gold. J Phys B: At Mol Phys 14:2321–2327
37. Migdalek J (1978) Relativistic oscillator strengths for some transitions in Cu(I), Ag(I) and Au(I). J Quant Spectrosc Radiat Transfer 20:81–87
38. Migdałek J (1976) Theoretical oscillator strengths III. Transitions in Au I, Hg II, Pb IV, and Bi V spectra. Can J Phys 54:2272–2278
39. Beideck DJ, Curtis LJ, Irving RE, Maniak ST, Hellborg R, Johansson SG, Martinson I, Rosberg M (1993) J Opt Soc Am B 10:977–981
40. Bielski A (1975) A critical survey of atomic transition probabilities for CuI. J Quant Spectrosc Radiat Transfer 15:463–472
41. NIST database. http://physics.nist.gov/PhysRefData/ASD/lines_form.html
42. Aguilera JA, Aragon C (2007) Apparent excitation temperature in laser-induced plasma. J Phys Conf Ser 59:210–217

43. Aguilera JA, Aragon C (2004) Characterization of a laser-induced plasma by spatially resolved spectroscopy of neutral atom and ion emissions. Comparison of local and spatially integrated measurements. Spectrochim Acta Part B 59:1861–1876
44. Konjevic N (1990) Experimental Stark widths and shifts for spectral lines of neutral and ionized atoms. J Phys Chem Ref Data 31:3
45. Dimitrijevic MS, Brechot SS (2003) Stark broadening of AgI spectral lines. At Data Nucl Data Tables 85:269–290
46. Gigososa MA, Gnzalezb MA, Cardenoso V (2003) Computer simulated Balmer-alpha, -beta and -gamma Stark line profiles for non-equilibrium plasmas diagnostics. Spectrochim Acta Part B 58:1489–1504
47. Praher B, Palleschi V, Viskup R, Heitz J, Pedarnig JD (2010) Calibration free laser-induced breakdown spectroscopy of oxide materials. Spectrochim Acta Part B 65:671–679
48. Abbass Q, Ahmed N, Ahmed R, Baig MA (2016) A comparative study of calibration free methods for the elemental analysis by laser induced breakdown spectroscopy. Plasma Chem Plasma Process 36:1287–1299
49. Gomba JM, Angelo CD, Bertuccelli D (2001) Spectroscopic characterization of laser induced breakdown in aluminum lithium alloy samples for quantitative determination of traces. Spectrochim Acta Part B 56:695–705
50. Tawfik W, Mohamed Y (2008) Improved LIBS limit of detection of Be, Mg, Si, Mn, Fe and Cu in aluminum alloy samples using a portable Echelle spectrometer with ICCD camera. Opt Laser Technol 40:30–38
51. Drogoff L, Margotb J, Chakera M, Sabsabi M, Barthelemy O, Johnstona T (2001) Temporal characterization of femtosecond laser pulses induced plasma for spectrochemical analysis of aluminum alloys. Spectrochim Acta Part B 56:987–1002
52. Ingle J, Crouch S, Lafferty K (1988) Spectrochemical analysis. Prentice Hall, New Jersey
53. Giacomo AD, Koral C, Valenza G, Gaudiuso R, Aglio MD (2016) Nanoparticle enhanced laser-induced breakdown spectroscopy for microdrop analysis at subppm level. Anal Chem 88:5251–5257